

MRI assessment of whole-brain structural changes in aging

Hui Guo,^{1,2} William Siu,^{1,3}
Ryan CN D'Arcy,^{1,4} Sandra E
Black,^{5,6} Lukas A Grajauskas,^{1,4}
Sonia Singh,^{7,8} Yunting Zhang,²
Kenneth Rockwood,^{9,10}
Xiaowei Song^{1,4,9}

On behalf of The Alzheimer's
Disease Neuroimaging Initiative
and the National Alzheimer's
Coordinating Center

¹Health Sciences and Innovation, ImageTech Laboratory, Fraser Health Authority, Surrey, BC, Canada; ²Department of Diagnostic Imaging, Tianjin Medical University General Hospital, Tianjin, China; ³Department of Medical Imaging, Fraser Health Authority, Surrey; ⁴Departments of Applied Sciences and Computing Science, Simon Fraser University, Burnaby, BC; ⁵Department of Medicine (Neurology); ⁶LC Campbell Cognitive Neurology Research Unit, Hurvitz Brain Sciences Research Program, Sunnybrook Research Institute, Sunnybrook Health Sciences Centre & University of Toronto, Toronto, ON; ⁷Department of Family Medicine, University of British Columbia, Vancouver, BC; ⁸Department of Research and Evaluation, Fraser Health, Surrey, BC; ⁹Department of Medicine (Geriatric Medicine), Dalhousie University; ¹⁰Centre for Healthcare of the Elderly, Nova Scotia Health Authority, Halifax, NS, Canada

Correspondence: Xiaowei Song
Health Sciences and Innovation,
ImageTech Laboratory, Fraser Health
Authority, 13750 96th Avenue, Surrey,
BC, Canada
Tel +1 640 585 5666 ext 774986
Fax +1 604 580 4925
Email xiaowei.song@fraserhealth.ca

Purpose: One of the central features of brain aging is the accumulation of multiple age-related structural changes, which occur heterogeneously in individuals and can have immediate or potential clinical consequences. Each of these deficits can coexist and interact, producing both independent and additive impacts on brain health. Many of the changes can be visualized using MRI. To collectively assess whole-brain structural changes, the MRI-based Brain Atrophy and Lesion Index (BALI) has been developed. In this study, we validate this whole-brain health assessment approach using several clinical MRI examinations.

Materials and methods: Data came from three independent studies: the Alzheimer's Disease Neuroimaging Initiative Phase II (n=950; women =47.9%; age =72.7±7.4 years); the National Alzheimer's Coordinating Center (n=722; women =55.1%; age =72.7±9.9 years); and the Tianjin Medical University General Hospital Research database on older adults (n=170; women =60.0%; age =62.9±9.3 years). The 3.0-Tesla MRI scans were evaluated using the BALI rating scheme on the basis of T1-weighted (T1WI), T2-weighted (T2WI), T2-weighted fluid-attenuated inversion recovery (T2-FLAIR), and T2*-weighted gradient-recalled echo (T2*GRE) images.

Results: Atrophy and lesion changes were commonly seen in each MRI test. The BALI scores based on different sequences were highly correlated (Spearman $r^2 > 0.69$; $P < 0.00001$). They were associated with age ($r^2 > 0.29$; $P < 0.00001$) and differed by cognitive status ($\chi^2 > 26.48$, $P < 0.00001$). T2-FLAIR revealed a greater level of periventricular ($\chi^2 = 29.09$) and deep white matter ($\chi^2 = 26.65$, $P < 0.001$) lesions than others, but missed revealing certain dilated perivascular spaces that were seen in T2WI ($P < 0.001$). Microhemorrhages occurred in 15.3% of the sample examined and were detected using only T2*GRE.

Conclusion: The T1WI- and T2WI-based BALI evaluations consistently identified the burden of aging and dementia-related decline of structural brain health. Inclusion of additional MRI tests increased lesion differentiation. Further research is to integrate MRI tests for a clinical tool to aid the diagnosis and intervention of brain aging.

Keywords: aging, brain atrophy and lesion index (BALI), brain health, MRI pulse sequences, structural brain changes

Introduction

Brain aging is associated with multiple structural changes, many of which can be visualized using MRI. Combinations of brain atrophy, small vessel changes, microbleeds, white matter hyperintensities, and impaired white matter integrity occur commonly in older adults.¹⁻⁴ Medial temporal lobe atrophy (MTA) is a hallmark change for Alzheimer's disease,^{5,6} and shrinkage of cortical regions and enlargement of the ventricles are particularly predictive of dementia progression.⁷ The degrees of atrophy, lacunar infarcts, and white matter hyperintensity can be correlated,^{1,3,8} and vascular

and white matter changes in mid-adulthood can lead to a more severe white matter burden and a higher atrophy rate, increasing the risk of dementia later in life.^{7–12} Noting the interaction between these deficits, the study of brain aging clearly requires an approach that allows for an integrated evaluation of structural brain changes.

While the additive effects of the multiple structural changes that present in the aging brain has been noted, there is a significant gap in our understanding of the interaction and consequences of these changes. To address this gap, we pioneered the Brain Atrophy and Lesion Index (BALI) approach.^{13–15} By adapting several widely used rating schemes, each of which focuses on one aspect of brain change (eg, atrophy and white matter hyperintensity^{5,16,17}), we created an index that assesses structural degeneration across the entire brain. The BALI evaluates changes in seven categories and summarizes the categorical sub-scores into a total score.^{14,15,18} The first category includes gray matter lesions (cortical infarcts), subcortical lesions, and subcortical dilated perivascular spaces (GM-SV). Subsequent categories assess deep white matter lesions (DWM), periventricular white matter lesions (PV), lesions in the basal ganglia and surrounding areas (BG), lesions in the infratentorial compartment (IT), and global atrophy (GA). An “other findings” category records changes such as neoplasm, trauma, and malformations, and hydrocephalus. This approach recognizes that some changes may have little clinical consequence when considered on their own; however, building on a deficit accumulation approach, even small deficits can sum to create clinically relevant – and statistically significant – effects.¹⁹

Supporting the utility of this approach, previous publications have shown BALI scores to be significantly related to age and dementia progression, and easy to use, as BALI can be readily learned and quickly scored.^{14,15,20–22} As with several other MRI rating systems, the BALI has high intra- and inter-rater reliability, comparable to that seen with time-consuming volumetric measurements.^{23–26} While some newer whole-brain approaches are emerging, they lack the breadth of the BALI, targeting either atrophy²³ or white matter changes.²⁴ As an integrative measure of age-related brain structural deficits, the BALI has shown characteristic dynamics, similar to those seen with other age-related deficit accumulation measures, such as the frailty index, and cognitive test scores.^{21,22,27}

While early iterations of the BALI evaluation used only 3D T1- and T2-weighted images (T1WI and T2WI), which are commonly acquired in research protocols, clinical MR examinations often include other image types. For

example, T2-weighted fluid-attenuated inversion recovery sequence (T2-FLAIR) is used to differentiate between cerebrospinal fluid and subtle lesions,²⁸ and T2*-weighted gradient recalled echo sequence (T2*GRE) is used to detect microhemorrhages.²⁹ Here, we conducted this study to validate the BALI using these four routine clinical MRI sequences. Our interest was to understand if these clinical MRI sequences could be applied independently, and in combination, to improve the evaluation of age-related common brain structural changes using BALI. Our objective was to determine how the BALI assessment could be improved by employing multiple clinical MRI tests. To assess the generalizability of the result, we conducted this study using three independent MRI datasets (total N=1,791).

Materials and methods

Data

Three datasets were used with permission: the Alzheimer’s Disease Neuroimaging Initiative (ADNI), the National Alzheimer’s Coordinating Center (NACC) Uniform Data Set (UDS), and the Tianjin Medical University Research dataset (TMUGHR).

1. The ADNI was launched in 2003 as a public–private partnership, led by Principal Investigator Michael W Weiner, MD. The primary goal of ADNI has been to test whether serial MRI, positron emission tomography (PET), biological markers, and clinical and neuropsychological assessment can be combined to measure the progression of mild cognitive impairment (MCI) and early Alzheimer’s disease (AD). Participants who were randomized for 3.0T scans were first screened at 1.5T for the inclusion/exclusion criteria.^{30,31} For up-to-date information, see www.adni-info.org. The present study examined ADNI Phase II subjects at baseline (n=950; women =47.9%; age =72.7±7.4 years; Table 1), which included subjects with normal cognition (NC), mild cognitive impairment (MCI), and Alzheimer’s disease (AD). Each participant had 3D T1WI at 3.0T. Among the subjects, 944 also had T2*GRE and 276 had T2 FLAIR, while no one had all four tests. All images were reviewed to identify and score brain changes; T1WI BALI scores were constructed for all subjects and used to correlate with age and cognitive status.
2. The NACC UDS was funded by the National Institute of Aging to facilitate data sharing from 34 Alzheimer’s Disease Centers (ADCs) across the USA.^{32,33} The NACC database contained both research samples and clinical samples from different protocols of the ADCs without

Table 1 Characteristics of the datasets

Dataset	ADNI			NACC			TMUGHR		
Diagnosis	NC	MCI	AD	NC	MCI	Dementia	NC	MCI	AD
N	311	486	153	385	186	151	120	30	20
Age (years)	73.4±6.3	71.7±7.5	74.8±8.2	70.3±10.9	75.4±7.7	75.7±7.9	61.6±9.6	66.3±8.3	66.1±6.6
Female (%)	54.0	45.7	42.5	66.0	35.5	42.4	60.8	60.0	55.0
Education (years)	16.6±2.5	16.2±2.7	15.8±2.1	16.0±2.7	15.5±2.8	14.9±3.1	13.5±3.4	12.0±3.5	10.2±3.9
CDR (0–3)	0.0±0.0	0.5±0.0	0.8±0.3	0.0±0.1	0.2±0.1	0.4±0.2	0.0±0.1	0.2±0.2	0.6±0.2
MMSE (0–30)	29.0±1.3	28.0±1.7	23.1±2.1	29.1±1.2	26.4±2.5	20.6±5.0	28.8±1.0	27.0±0.5	24.3±2.0

Note: Data are presented as mean ± SD, unless otherwise as indicated.

Abbreviations: AD, Alzheimer's disease; ADNI, Alzheimer's disease neuroimaging initiative; CDR, clinical dementia rating; MCI, mild cognitive impairment; MMSE, Mini-Mental State Examination; N, number of subjects; NACC, National Alzheimer's Coordinating Center; NC, normal cognition; TMUGHR, Tianjin Medical University Research dataset.

NACC's input in the study designs. For this study, the UDS portion of the NACC data were retrieved, and baseline data from people aged ≥ 55 years that were collected and submitted to NACC between September 2005 and January 2015 were used, which involved seven ADCs. These included subjects with NC, MCI, and AD or other dementia diagnoses ($n=722$; women =55.1%; age =72.7±9.9 years; Table 1). Subjects who were known to be in ADNI were excluded prior to data release by NACC; however, some ADNI cases may be included in NACC if the information regarding their ADNI participation was missing. Imaging data collection and acquisition protocols varied by ADC. All subjects in the present study had a high-resolution 3D T1WI at 3T, of whom 660 also had T2-FLAIR, 262 had T2WI, and 9 had T2*GRE, while no one had all four images. All images were reviewed to identify and score brain changes; T1WI BALI scores were constructed for all subjects and used to correlate with age and cognitive status.

3. TMUGHR data were obtained from the imaging database of research protocols conducted at TMUGHR's Diagnostic Imaging Department between December 2015 and June 2016. MRI images of participants who were aged ≥ 50 years with no neurologic disorders other than designated cognitive diagnosis were used in the study ($n=170$; women =60.0%; age =62.9±9.3 years, including subjects with NC, MCI, and early AD; Table 1). All the participants had a 3.0T MRI scan using all four sequences.

Before being made available for public access, the MRI scans of the ADNI and NACC datasets underwent quality control checks, excluding subjects with structural abnormalities and/or having an image with common scan artifacts from the data sources.^{30,33} Upon receiving data, the images were reviewed and evaluated for structural brain changes,

consistently applying the semiquantitative BALI rating schema (Figure S1A–D).^{15,18}

MRI tests

Table S1 summarizes the basic features of the four MRI sequences. In the datasets studied here, T1WI used IR-SPGR or MPRAGE, repetition time (TR)/echo time (TE) =2,300–3,000/3 ms, time of inversion (TI) =400–1,100 ms, flip angle =7°–11°, slice thickness =1.0–1.2 mm, FOV =26–27 cm, matrix =256×256, NEX =1. The T2WI used TR/TE =3,000–5,500/90–99 ms, flip angle =90° or 150°, slice thickness =3 mm, FOV =26 cm, matrix =256×256, NEX =3. The T2-FLAIR-based BALI rating used TR/TE =9,000–11,000/90–147 ms, TI =2,250–2,500 ms, flip angle =150°, slice thickness =3.0–5.0 mm, FOV =26 cm, matrix 256×256, NEX =2. The T2*GRE-based BALI rating used TR/TE =650–800/3–20 ms, flip angle =20°, slice thickness =3.0–4.0 mm, FOV =26–30 cm, matrix =256×192–256, NEX =2.

BALI evaluation

The BALI rating schema was used to assess age-related changes in the brain by evaluating seven categories, assigning a value between 0 and 3 to each category to represent the severity of a change, a higher score meaning greater severity.^{14,15,18} In two categories (DWM and GA), values of 0–5 were used, allowing capture of more severe changes and thereby avoiding ceiling effects. In addition, a hemorrhage category was evaluated, assigning a value between 0 and 3. The BALI total score was calculated as the sum of the subscores of all the eight categories on the basis of the same sequence (eg, T1WI) or an algorithm combining the categorical scores of different sequences, with a possible maximum BALI total score of 28. Two experienced neuro-radiologists performed the evaluation following the BALI

rating schema (Figures S1 and S2).^{15,18} One person evaluated and scored all the images, and the other assessed a randomly selected 20% images for inter-rater agreement tests. Different MRI sequences were assessed separately in random order on different days to minimize possible recall bias. Five other qualified BALI raters who were trained with the method participated in the T1WI rating of the ADNI and NACC datasets. Different raters reviewed and scored the images independently, blinded to the information concerning the subject demographics, diagnosis, and cognitive test results.

Analysis

All images from the three datasets were reviewed for the identification and scoring of brain changes assessed using BALI. Images representing changes in each BALI category were selected (including those in Figures 1–3; Figures S1 and S2). Statistical analyses correlating BALI scores with age and cognitive status (eg, the Mini-Mental State Examination [MMSE]) used T1WI in ADNI and NACC datasets and each of the sequences of the TMUGHR dataset. Analyses comparing the performance of the MRI sequences were conducted on the BALI total and categorical scores using the TMUGHR dataset. Inter-rater reliability of scoring was assessed for each BALI total score and sub-categorical score using a 20% random subsample, evaluated by two raters. Intrarater reliability was also assessed, for which a 20% random subsample was evaluated twice by a same rater on separate days. In each case, an intraclass correlation coefficient (ICC) was calculated for the absolute agreement rate, with both sample and rater as random factors. Nonparametric tests used the Kruskal–Wallis two-sample χ^2 for the differences in the group mean BALI total score and subscores, and the Spearman correlation coefficient was used for examining the associations between different sequences and the relationships of the BALI score with age and cognitive assessment measurements. All statistical analyses were performed using IBM Statistics SPSS version 23.

Ethics

The respective ethics boards of study centers of the original research projects approved the data collection protocols; all the subjects who participated in the projects provided informed consent form. Additional ethical approvals for the analyses were obtained from the Fraser Health (FHREB 2014–083, 2015–030) and the Tianjin Medical University Research Ethics Boards (TMUREB 2014–0311). All data used in the analyses had been de-identified.

Results

Atrophic and lesion-based changes in the various BALI categories were consistently shown in each MRI sequence (Figure S1). The BALI scores differed by sequences ($\chi^2=21.38$, $P<0.001$; Table 2), but were well correlated ($r^2>0.69$; $P<0.00001$; Table 3; $n=170$). Each BALI score differed by diagnosis ($\chi^2=26.48$, $n=950$ for ADNI; $\chi^2=41.89$, $n=722$ for NACC; $\chi^2>27.77$, $n=170$ for TMUGHR; $P<0.001$; Table 2). The BALI was also highly correlated with age ($r^2=0.29$, $n=950$ for ADNI; $r^2=0.31$, $n=722$ for NACC; $r^2>0.25$, $n=170$ for TMUGHR; $P<0.00001$) and with the MMSE score ($r^2=0.11$, $n=950$ for ADNI; $r^2=0.14$, $n=722$ for NACC; $r^2>0.27$, $n=170$ for TMUGHR; $P<0.00001$).

The intrarater ICCs for the BALI total score ranged between 0.87 (95% CI =0.79–0.92) and 0.93 (95% CI =0.84–0.97), while the inter-rater ICCs ranged between 0.81 (95% CI =0.72–0.89) and 0.91 (95% CI =0.81–0.95). These moderately high reliability measures were compatible across datasets and sequences. The inter-rater ICCs of the categorical scores varied from 0.63 (0.38–0.79 with T1WI DWM) to 0.90 (0.91–0.95 with T2WI GMSV).

T2-FLAIR showed more lesions in the PV ($\chi^2=29.09$, $P<0.001$) and DWM ($\chi^2=26.65$, $P<0.001$), compared to T2WI or T1WI (Figure 1). Small patchy white matter lesions in the subcortical region were seen in T2-FLAIR, which were not always seen in T1WI or T2WI. The larger dilated perivascular spaces and lacunar malacia were more clearly differentiated on T2-FLAIR, but it missed small dilated perivascular spaces in multiple sites, including the cerebral peduncle of IT ($\chi^2>44.88$, $P<0.001$, $n=170$; Figure 1).

T2*GRE was not as sensitive as either T2WI or T1WI in evaluating many BALI categories ($\chi^2<3.35$; $P>0.067$; $n=170$). However, T2*GRE showed microhemorrhages in 15.3% of the sample, which were not seen in any other sequences (Figures 2 and 3). Hemosiderin deposition surrounding malacia lesions and calcification in the basal ganglia regions were also seen in T2*GRE (Figure 2).

Subjects with changes in the “Others” category were seen in 10.5% of the TMUGHR sample consistently using each sequence, which were rarely found in the ADNI (0.6%; $n=950$) or NACC (3.0%; $n=722$) sample, presumably related to scan checking prior to data release. These changes mainly consisted of <0.5 mm lacunar malacia, normal pressure hydrocephalus, cavernous malformation, and meningioma (Figure S2).

Table 4 lists the applicability of the sequences to scoring each BALI category, following which a combined

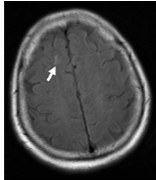
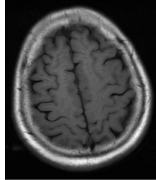
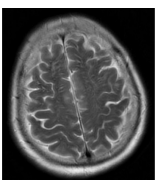
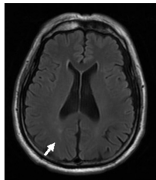
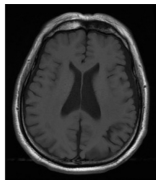
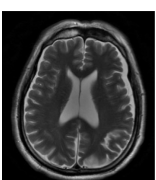
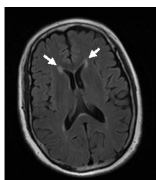
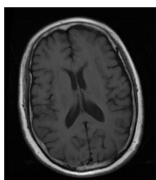
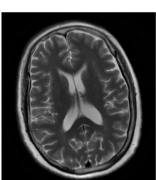
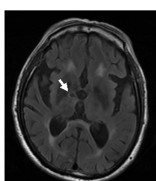
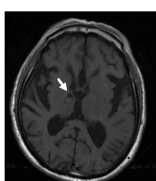
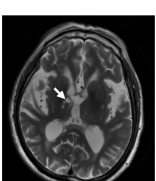
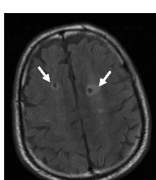
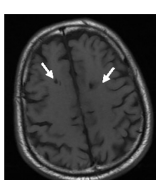
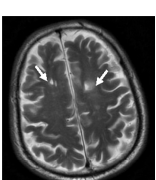
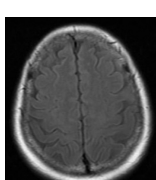
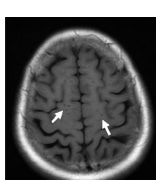
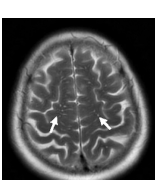
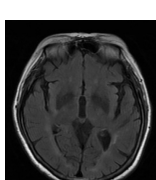
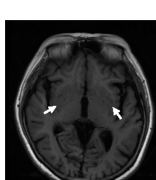
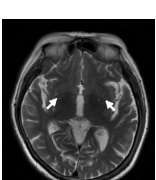
Lesions		Sequence		
		T2-FLAIR	T1WI	T2WI
White matter lesion	A			
	B			
	C			
Lacunar malacia	D			
	E			
Dilated perivascular spaces	F			
	G			

Figure 1 Examples of the characteristic changes shown on T2-FLAIR in comparison with those shown on T1WI and T2WI.

Notes: T2-FLAIR is comparatively more sensitive in detecting white matter lesions as shown in subcortical white matter (**A**), deep white matter (**B**), and periventricular white matter (**C**). Lacunar malacia in multiple regions are also seen more clearly on T2-FLAIR (**D**, **E**), shown as lower signal intensity in the central part surrounded by high signal intensity. In contrast, compared to T1WI and T2WI, the dilated perivascular spaces located in multiple sites are not seen on T2FLAIR, for example, in the subcortical region (**F**), and basal ganglia and surrounding region (**G**).

Abbreviations: T1WI, T1-weighted image; T2WI, T2-weighted image; T2-FLAIR, T2-weighted fluid-attenuated inversion recovery.

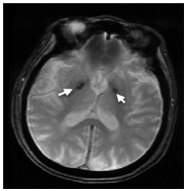
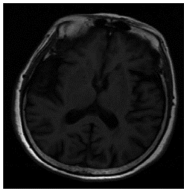
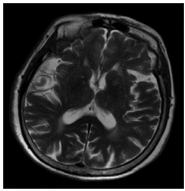
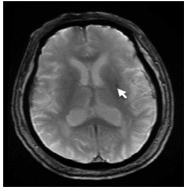
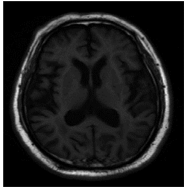
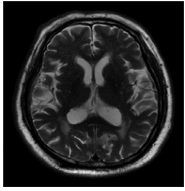
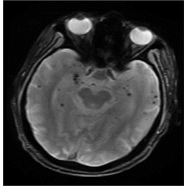
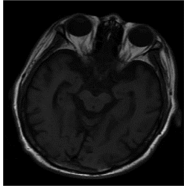
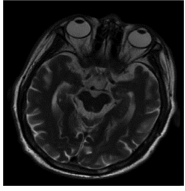
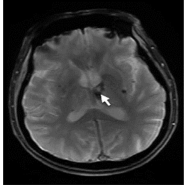
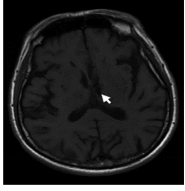
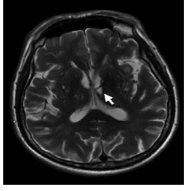
Lesions	Sequence		
	T2*GRE	T1WI	T2WI
A Calcification			
B Microhemorrhage			
C Multiple microhemorrhages			
D Malacia with hemosiderin deposition			

Figure 2 Examples of the characteristic changes shown on T2*GRE in comparison with those shown on T1WI and T2WI.
Notes: Changes of each BALI category are less reliably identified on T2*GRE than on T2WI or T1WI. Susceptive lesions are more sensitively revealed on T2*GRE, for example, calcification (A), microhemorrhage (B), multiple microhemorrhages (C), and malacia with hemosiderin deposition (D).
Abbreviations: BALI, brain atrophy and lesion index; T1WI, T1-weighted image; T2WI, T2-weighted image; T2*GRE, T2*-weighted gradient recalled echo sequence.

BALI score was constructed using T2WI for GMSV, BG, IT, and others; T2FLAIR for DWM and PV; T1WI for GA; and GRE for hemorrhage. The combined score showed a marginal but insignificant increase in the

inter-rater ICC (0.86; 95% CI=0.79–0.93) and correlation coefficient with age ($r^2=0.27$) and with MMSE ($r^2=0.33$; $P<0.00001$; $n=170$; Tables 3 and 4), compared to T1WI and T2WI.

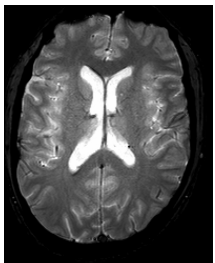
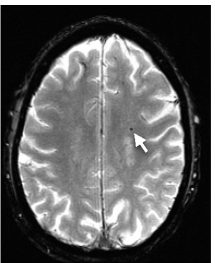
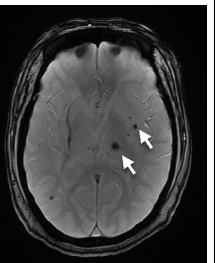
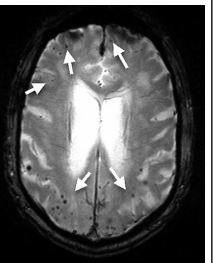
T2*GRE	Score			
	0	1	2	3
Microhemorrhage	None	Only one	More than one	Many
				

Figure 3 Microhemorrhage on T2*GRE at 3.0T.
Note: A score between 0 and 3 is given to grade the severity of microhemorrhage, which can range from clear to one, multiple, and diffused spots.
Abbreviation: T2*GRE, T2*-weighted gradient recalled echo sequence.

Table 2 The categorical and total scores of the Brain Atrophy and Lesion Index (BALI) by diagnosis

Diagnosis	ALL	NC	MCI	AD	K-W/ χ^2 (P)
N		120	30	20	
GM-SV					
T1WI	1.3±0.6	1.2±0.6	1.6±0.5	1.9±0.7	19.91 (<0.0001)
T2WI	1.8±0.5	1.7±0.5	1.9±0.3	2.2±0.5	17.45 (<0.0001)
T2-FLAIR	1.4±0.6	1.4±0.6	1.4±0.6	1.8±0.8	5.10 (0.078)
T2*GRE	1.6±0.6	1.5±0.5	1.7±0.4	2.1±0.6	20.09 (<0.0001)
K-W/ χ^2 (P)	55.12 (<0.0001)				
DWM					
T1WI	1.6±0.8	1.5±0.7	1.9±0.7	2.2±0.8	18.08 (<0.0001)
T2WI	1.9±0.6	1.8±0.7	2.2±0.6	2.4±0.5	17.80 (<0.0001)
T2-FLAIR	2.0±0.7	1.9±0.7	2.4±0.5	2.5±0.5	19.41 (<0.0001)
T2*GRE	1.8±0.8	1.7±0.8	2.2±0.6	2.4±0.6	21.70 (<0.0001)
K-W/ χ^2 (P)	26.65 (<0.0001)				
PV					
T1WI	1.2±0.8	1.0±0.7	1.2±0.8	1.8±0.9	12.55 (0.002)
T2WI	1.4±0.8	1.2±0.7	1.5±0.9	2.1±0.9	21.09 (<0.0001)
T2-FLAIR	1.7±0.9	1.5±0.9	2.0±0.9	2.3±0.9	12.76 (0.002)
T2*GRE	1.3±0.9	1.1±1.0	1.5±0.9	2.1±0.9	21.47 (<0.0001)
K-W/ χ^2 (P)	29.09 (<0.0001)				
BG					
T1WI	2.0±0.4	2.0±0.4	2.0±0.2	2.2±0.4	3.27 (0.195)
T2WI	2.0±0.5	1.9±0.5	2.1±0.3	2.4±0.5	17.90 (<0.0001)
T2-FLAIR	1.9±0.6	1.8±0.7	2.1±0.3	2.2±0.4	12.21 (0.002)
T2*GRE	2.1±0.5	2.0±0.6	2.2±0.4	2.4±0.5	10.16 (0.006)
K-W/ χ^2 (P)	11.05 (0.011)				
IT					
T1WI	1.1±0.9	0.9±0.9	1.4±0.8	2.0±0.7	23.19 (<0.0001)
T2WI	1.4±0.9	1.2±1.0	1.8±0.6	2.1±0.6	22.87 (<0.0001)
T2-FLAIR	1.1±1.0	1.0±1.0	1.3±1.0	1.7±0.9	9.31 (0.010)
T2*GRE	1.7±0.8	1.6±0.9	1.9±0.6	2.1±0.6	7.97 (0.019)
K-W/ χ^2 (P)	48.88 (<0.0001)				
GA					
T1WI	1.0±0.9	0.8±0.7	1.1±0.8	2.1±1.1	27.24 (<0.0001)
T2WI	1.0±0.9	0.8±0.8	1.3±1.0	2.1±1.0	28.79 (<0.0001)
T2-FLAIR	1.0±0.9	0.8±0.8	1.2±0.8	2.0±1.0	24.43 (<0.0001)
T2*GRE	1.2±1.0	1.0±0.9	1.3±1.0	2.2±0.9	23.24 (<0.0001)
K-W/ χ^2 (P)	3.83 (0.280)				
Others					
T1WI	0.1±0.5	0.1±0.3	0.1±0.3	0.5±0.8	5.88 (0.053)
T2WI	0.1±0.5	0.1±0.3	0.1±0.3	0.5±0.8	6.55 (0.040)
T2-FLAIR	0.1±0.4	0.1±0.3	0.1±0.3	0.5±0.8	8.14 (0.017)
T2*GRE	0.1±0.4	0.1±0.3	0.1±0.3	0.5±0.8	8.00 (0.018)
K-W/ χ^2 (P)	0.44 (0.932)				
Hemorrhage					
T1WI	–	–	–	–	
T2WI	–	–	–	–	
T2-FLAIR	–	–	–	–	
T2*GRE	0.2±0.6	0.1±0.4	0.3±0.7	0.6±0.9	9.10 (0.011)
Total					
T1WI	8.4±03.0	7.5±2.5	9.4±1.9	12.5±3.5	40.54 (<0.0001)
T2WI	9.7±3.0	8.7±2.5	10.9±2.0	13.6±3.4	42.17 (<0.0001)
T2-FLAIR	9.3±3.3	8.5±3.0	10.2±2.0	12.8±3.9	27.77 (<0.0001)
T2*GRE	9.9±3.4	9.0±3.1	10.9±2.2	13.7±3.3	32.08 (<0.0001)
Combined ^a		9.0±2.4	10.9±1.9	13.9±3.7	39.94 (<0.0001)
K-W/ χ^2 (P)	21.38 (<0.0001)				

Notes: Data are presented as mean ± SD. ^aThe combined total score was constructed by integrating categorical scores evaluated using multiple MRI sequences: T2WI for GMSV, BG, IT, and others; T2FLAIR for DWM and PV; T1WI for GA; and GRE for hemorrhage. – indicates not visible.

Abbreviations: AD, Alzheimer's disease; BG, lesions in the basal ganglia and surrounding areas; DWM, deep white matter lesions; GA, global atrophy; GM-SV, gray matter and subcortical lesions – subcortical dilated perivascular spaces; IT, Lesions in the infratentorial compartment; K-W/ χ^2 , Kruskal-Wallis/Chi square; MCI, mild cognitive impairment; N, number of subjects; NC, normal cognition; PV, periventricular white matter lesions; T1WI, T1-weighted image; T2WI, T2-weighted image; T2-FLAIR, T2 fluid-attenuated inversion recovery; T2*GRE, T2*-weighted gradient recalled echo sequence.

Table 3 Correlation coefficients between sequence pairs for the Brain Atrophy and Lesion Index (BALI) total score

	T1WI	T2WI	T2-FLAIR	T2*GRE	Combined ^a
T1WI	1	0.94	0.83	0.86	0.90
T2WI		1	0.86	0.87	0.94
T2-FLAIR			1	0.89	0.86
T2*GRE				1	0.86
Combined ^a					1

Notes: ^aThe combined total score was constructed by integrating categorical scores evaluated using multiple MRI sequences: T2WI for GMSV, BG, IT, and others; T2-FLAIR for DWM and PV; T1WI for GA; and GRE for hemorrhage. For each test, n=170; level of significance $P<0.00001$.

Abbreviations: T1WI, T1-weighted imaging; T2WI, T2-weighted imaging; T2-FLAIR, T2-weighted fluid attenuation inversion recovery sequence; T2*GRE, T2*-weighted gradient recalled echo sequence.

Discussion

This study investigated the use of routine clinical MRI examinations in the evaluation of brain health in older adults. The BALI was created to allow us to simultaneously assess multiple structural changes in the aging brain, addressing a challenging aspect in the study of brain aging, as these changes can coexist and interact to produce additive impacts on cognition.^{1,3,7-9,34} Classically, many changes are not considered clinically meaningful or pathologically indicative by themselves, especially when small in magnitude. Consequently, the impact of multiple, small-scale variations in an older individual has not been adequately investigated. For instance, the widely used Fazekas and Schelten scores are focused only on the assessment of white matter hyperintensity and the MTA, respectively.^{16,17} The few recent studies that have attempted to account for more than one type of change have not taken a whole-brain approach and do not include many of the changes that occur.^{23,24,35}

Table 4 Application of four routine clinical MRI sequences in the evaluation of the Brain Atrophy and Lesion Index (BALI)

BALI category	T1WI	T2WI	T2-FLAIR	T2*GRE
GM-SV	✓	✓*	✓–	✓–
WM	✓	✓	✓*	✓–
PV	✓	✓	✓*	✓–
BG	✓	✓	✓	–
IT	✓	✓*	✓–	–
GA	✓	✓	✓	✓
Others	✓	✓	✓	✓
Microhemorrhage	–	–	–	✓*

Notes: ✓*: most suitable; ✓: suitable; ✓–: unsuitable but possible; –: impossible.

Abbreviations: BG, lesions in the basal ganglia and surrounding areas; DWM, deep white matter lesions; GA, global atrophy; GM-SV, gray matter and subcortical lesions – subcortical dilated perivascular spaces; IT, lesions in the infratentorial regions; PV, periventricular white matter lesions; T1WI, T1-weighted imaging; T2WI, T2-weighted imaging; T2-FLAIR, T2-weighted fluid attenuation inversion recovery sequence; T2*GRE, T2*-weighted gradient recalled echo sequence.

It is of vital importance to investigate the cumulative effects of small changes, as generally aging is characterized by the accumulation of deficits. This can be quantified using clinically detectable health problems, as well as common laboratory tests and biomarkers. The BALI extends this approach to brain structure by adapting the evaluation schema of several existing rating scales and integrating the changes in a simple total score. Data of this study confirmed that the BALI is a robust tool that allows structural brain health assessment in relation to age, cognitive performance, and dementia diagnosis.^{13–15,18,20,21} Even though MRI scans are not the gold standard for assessing pathology in brain tissue, their use is uniquely suited for in vivo detection of neuropathological changes of the whole brain to aid in early diagnosis and treatment.^{2,7,36}

Developed initially as a research tool, BALI scoring using 3D T1WI (and also T2WI) has been consistently verified across multiple datasets. The 3D T1WI is most commonly used in research datasets, with excellent brain tissue contrast and great spatial resolution. When the approach is extended to include T2-FLAIR and T2*GRE images^{28,29} – both common clinical sequences – several changes are better differentiated. As shown in the results, adding more MRI tests in BALI rating could improve the sensitivity of the assessment through increased differentiation of the signal of normal tissue and abnormal structures.^{28,29} With this implemented, T2WI is ideal for scoring the gray matter, subcortical lesions, and infratentorial lesions categories. T2-FLAIR is best for changes in the DWM, and PV categories (noting that in T2-FLAIR, thin-line hyperintensity surrounding the ventricles was always present and should not be mistaken with the pencil thin line with the evaluation). T1WI, T2WI, and T2-FLAIR are all suitable for the basal ganglia and surrounding areas, and the GA category, while T1WI or T2WI are most suitable for malacia, and changes of the “Others” category. Additionally, T2*GRE is optimal for detecting microbleeds, although it is not reliable to score other BALI categories due to a patchy low signal intensity associated with normal deposition of paramagnets or flow artifacts.

The study showed that employing more images within our BALI evaluation improved the differentiation of brain changes, enhancing its applicability. Examples included the detection of subcortical white matter changes using T2-FLAIR and detection of lacunes with hemosiderin deposition or microbleeds using T2*GRE. The latter is of an increasingly greater interest in aging research, as the early presentation, high prevalence, and marked impact of microhemorrhage in older population are increasingly recognized. A recent report, based on a large-scale MRI study with

multiple follow-ups, revealed that vascular changes are the very first structural brain changes leading to AD.³⁴ Inclusion of microhemorrhage in BALI assessment may help earlier identification of those most at risk.

The study also has some limitations. The datasets are not community based, and therefore do not represent the general population. It is possible that the changes shown in the participants did not cover the full range of possible changes in the older adults' brain. Typically, study participants are categorized into groups to represent healthy aging, cognitive decline, and AD, and participants are screened to exclude other neurological conditions such as stroke and brain tumors. Possibly related to the scan checking and exclusion, only a small subsample of the multicenter datasets has scored non-zero for the "Others" category, which evaluates clinically significant changes. Also, two datasets were from large-scale multicenter studies, in which subject inclusion criteria and/or image acquisition protocols can vary by study center, leading to potential difference in the rating score. Caution should be taken to rule out such influence before data are to be pooled for analysis. Standardization for data procedures across study centers can be beneficial. Finally, it is challenging to correctly optimize the weighting of the BALI subscores while retaining the generalizability for assessing brain aging, as each deficit may contribute to cognitive decline differently. Even with these limitations, the study demonstrated that whole-brain changes in aging are generalized in different samples.

An apparent question about using multiple MRI examinations in the BALI rating is the time required to process the many images. The T1WI or T2WI BALI scoring takes just a few minutes to complete,¹⁸ allowing it to serve as a fast rating tool, ensuring ease of application in busy clinical settings. While introducing additional sequences improves the sensitivity of the index, scoring additional images would require a much longer rating time. The need for rater expertise with multiple sequences may also present an additional challenge. Effectively dealing with this increased workload will rely on computer-aided solutions. This need is motivating our ongoing research to develop an optimized algorithm, which will allow automated uni- and multisequence-based BALI assessments.

Conclusion

The T1WI- and T2WI-based evaluations consistently captured deficits in each BALI category, reflecting the burden of age- and disease-related whole-brain structural changes in older adults. T2-FLAIR and T2*GRE improved the detection of white matter and microhemorrhage changes, enhancing the assessment. The study supports an automated

BALI integration of multiple routine MRI scans, laying the groundwork for a future clinical tool to support brain aging diagnosis and intervention.

Acknowledgments

This research received funding support from Canadian Institutes of Health Research (CSE125739), National Nature Science Foundation of China (81401379), and Surrey Hospital & Outpatient Centre Foundation. KR was supported by Dalhousie Medical Research Foundation as Kathryn Allen Weldon Chair in Alzheimer Research. The authors would acknowledge Y Shi, S Peng, N Dhindsa, and S Merchant for assistance with data acquisition, processing, and analysis; B Chinda with author-proofreading.

Data used in the preparation of this article were partially obtained with permission from the Alzheimer's Disease Neuroimaging Initiative (ADNI) database (adni.loni.usc.edu) and the National Alzheimer's Coordinating Center (NACC) Uniform Data Set (www.alz.washington.edu). As such, the investigators within the ADNI and the NACC contributed to the design and implementation of ADNI and NACC and/or provided data but did not participate in analysis or writing of this report.

The ADNI data collection and sharing was funded by the ADNI (National Institutes of Health [NIH] Grant U01 AG024904) and DOD ADNI (Department of Defense award number W81XWH-12-2-0012). ADNI is funded by the National Institute on Aging (NIA) and the National Institute of Biomedical Imaging and Bioengineering, and through generous contributions from the following: AbbVie, Alzheimer's Association; Alzheimer's Drug Discovery Foundation; Araclon Biotech; BioClinica, Inc.; Biogen; Bristol-Myers Squibb Company; CereSpir, Inc.; Cogstate; Eisai Inc.; Elan Pharmaceuticals, Inc.; Eli Lilly and Company; EuroImmun; F Hoffmann-La Roche Ltd and its affiliated company Genentech, Inc.; Fujirebio; GE Healthcare; IXICO Ltd.; Janssen Alzheimer Immunotherapy Research & Development, LLC.; Johnson & Johnson Pharmaceutical Research & Development LLC.; Lumosity; Lundbeck; Merck & Co., Inc.; Meso Scale Diagnostics, LLC.; NeuroRx Research; Neurotrack Technologies; Novartis Pharmaceuticals Corporation; Pfizer Inc.; Piramal Imaging; Servier; Takeda Pharmaceutical Company; and Transition Therapeutics. The Canadian Institutes of Health Research is providing funds to support ADNI clinical sites in Canada. Private sector contributions are facilitated by the Foundation for the NIH (www.fnih.org). The grantee organization is the Northern California Institute for Research and Education, and the study is coordinated by the

Alzheimer's Therapeutic Research Institute at the University of Southern California. ADNI data are disseminated by the Laboratory for Neuro Imaging at the University of Southern California. A complete listing of ADNI investigators can be found at: http://adni.loni.usc.edu/wp-content/uploads/how_to_apply/ADNI_Acknowledgement_List.pdf.

The NACC database is funded by NIA/NIH Grant U01 AG016976. NACC data are contributed by the NIA-funded ADCs: P30 AG019610 (PI Eric Reiman, MD), P30 AG013846 (PI Neil Kowall, MD), P50 AG008702 (PI Scott Small, MD), P50 AG025688 (PI Allan Levey, MD, PhD), P50 AG047266 (PI Todd Golde, MD, PhD), P30 AG010133 (PI Andrew Saykin, PsyD), P50 AG005146 (PI Marilyn Albert, PhD), P50 AG005134 (PI Bradley Hyman, MD, PhD), P50 AG016574 (PI Ronald Petersen, MD, PhD), P50 AG005138 (PI Mary Sano, PhD), P30 AG008051 (PI Steven Ferris, PhD), P30 AG013854 (PI M Marsel Mesulam, MD), P30 AG008017 (PI Jeffrey Kaye, MD), P30 AG010161 (PI David Bennett, MD), P50 AG047366 (PI Victor Henderson, MD, MS), P30 AG010129 (PI Charles DeCarli, MD), P50 AG016573 (PI Frank LaFerla, PhD), P50 AG016570 (PI Marie-Francoise Chesselet, MD, PhD), P50 AG005131 (PI Douglas Galasko, MD), P50 AG023501 (PI Bruce Miller, MD), P30 AG035982 (PI Russell Swerdlow, MD), P30 AG028383 (PI Linda Van Eldik, PhD), P30 AG010124 (PI John Trojanowski, MD, PhD), P50 AG005133 (PI Oscar Lopez, MD), P50 AG005142 (PI Helena Chui, MD), P30 AG012300 (PI Roger Rosenberg, MD), P50 AG005136 (PI Thomas Montine, MD, PhD), P50 AG033514 (PI Sanjay Asthana, MD, FRCP), P50 AG005681 (PI John Morris, MD), and P50 AG047270 (PI Stephen Strittmatter, MD, PhD).

Author contributions

HG and XS: study concept and design, research funding, and data access; HG, WS, and XS: first draft preparation; HG, WS, LG, and XS: imaging data management and evaluation, data processing, and statistical analysis; and all authors: result interpretation and various versions of manuscript editing and revising. All authors agreed upon the research finding and the publication of all the aspects in this paper.

Disclosure

The authors report no conflicts of interest in this work.

References

- Park JH, Seo SW, Kim C, et al. Pathogenesis of cerebral microbleeds: in vivo imaging of amyloid and subcortical ischemic small vessel disease in 226 individuals with cognitive impairment. *Ann Neurol*. 2013; 73(5):584–593.
- Prins ND, Scheltens P. White matter hyperintensities, cognitive impairment and dementia: an update. *Nat Rev Neurol*. 2015;11(3):157–165.
- Shim YS, Yang DW, Roe CM, et al. Pathological correlates of white matter hyperintensities on magnetic resonance imaging. *Dement Geriatr Cogn Disord*. 2015;39(1–2):92–104.
- Ramirez J, Berezuk C, McNeely AA, Gao F, McLaurin J, Black SE. Imaging the perivascular space as a potential biomarker of neurovascular and neurodegenerative diseases. *Cell Mol Neurobiol*. 2016;36(2): 289–299.
- Scheltens P, Leys D, Barkhof F, et al. Atrophy of medial temporal lobes on MRI in “probable” Alzheimer's disease and normal ageing: diagnostic value and neuropsychological correlates. *J Neurol Neurosurg Psychiatry*. 1992;55(10):967–972.
- McKhann GM, Knopman DS, Chertkow H, et al. The diagnosis of dementia due to Alzheimer's disease: recommendations from the National Institute on Aging-Alzheimer's Association workgroups on diagnostic guidelines for Alzheimer's disease. *Alzheimers Dement*. 2011;7(3): 263–269.
- Pacheco J, Goh JO, Kraut MA, Ferrucci L, Resnick SM. Greater cortical thinning in normal older adults predicts later cognitive impairment. *Neurobiol Aging*. 2015;36(2):903–908.
- Peng Y, Li S, Zhuang Y, et al. Density abnormalities in normal-appearing gray matter in the middle-aged brain with white matter hyperintense lesions: a DARTEL-enhanced voxel-based morphometry study. *Clin Interv Aging*. 2016;11:615–622.
- Boyle PA, Wilson RS, Yu L, et al. Much of late life cognitive decline is not due to common neurodegenerative pathologies. *Ann Neurol*. 2013; 74(3):478–489.
- Tosto G, Zimmerman ME, Carmichael OT, Brickman AM; Alzheimer's Disease Neuroimaging Initiative. Predicting aggressive decline in mild cognitive impairment: the importance of white matter hyperintensities. *JAMA Neurol*. 2014;71(7):872–877.
- Iturria-Medina Y, Sotero RC, Toussaint PJ, Mateos-Pérez JM, Evans AC; Alzheimer's Disease Neuroimaging Initiative. Early role of vascular dysregulation on late-onset Alzheimer's disease based on multifactorial data-driven analysis. *Nat Commun*. 2016;7:11934.
- Cai Z, Wang C, He W, et al. Cerebral small vessel disease and Alzheimer's disease. *Clin Interv Aging*. 2015;10:1695–1704.
- Chen W, Song X, Zhang Y, et al. An MRI-based semiquantitative index for the evaluation of brain atrophy and lesions in Alzheimer's disease, mild cognitive impairment and normal aging. *Dement Geriatr Cogn Disord*. 2010;30(2):121–130.
- Zhang N, Song X, Zhang Y, et al. An MRI brain atrophy and lesion index to assess the progression of structural changes in Alzheimer's disease, mild cognitive impairment, and normal aging: a follow-up study. *J Alzheimers Dis*. 2011;26(Suppl 3):359–367.
- Guo H, Song X, Vondorp R, et al. Evaluation of common structural brain changes in aging and Alzheimer disease with the use of an MRI-based brain atrophy and lesion index: a comparison between T1WI and T2WI at 1.5T and 3T. *AJNR Am J Neuroradiol*. 2014;35(3): 504–512.
- Fazekas F, Chawluk JB, Alavi A, Hurtig HI, Zimmerman RA. MR signal abnormalities at 1.5 T in Alzheimer's dementia and normal aging. *AJR Am J Roentgenol*. 1987;149(2):351–356.
- Scheltens P, Barkhof F, Leys D, et al. A semiquantitative rating scale for the assessment of signal hyperintensities on magnetic resonance imaging. *J Neurol Sci*. 1993;114(1):7–12.
- Guo H, Song X, Schmidt MH, et al. Evaluation of whole brain health in aging and Alzheimer's disease: a standard procedure for scoring an MRI-based brain atrophy and lesion index. *J Alzheimers Dis*. 2014; 42(2):691–703.
- Mitnitski A, Song X, Rockwood K. Assessing biological aging: the origin of deficit accumulation. *Biogerontology*. 2013;14(6):709–717.
- Zhang N, Song X, Zhang Y; Alzheimer's Disease Neuroimaging Initiative. Combining structural brain changes improves the prediction of Alzheimer's disease and mild cognitive impairment. *Dement Geriatr Cogn Disord*. 2012;33(5):318–326.

21. Song X, Mitnitski A, Zhang N, Chen W, Rockwood K; Alzheimer's Disease Neuroimaging Initiative. Dynamics of brain structure and cognitive function in the Alzheimer's disease neuroimaging initiative. *J Neurol Neurosurg Psychiatry*. 2013;84(1):71–78.
22. Mitnitski A, Song X, Rockwood K. Trajectories of changes over twelve years in the health status of Canadians from late middle age. *Exp Gerontol*. 2012;47(12):893–899.
23. Jang JW, Park SY, Park YH, et al. A comprehensive visual rating scale of brain magnetic resonance imaging: application in elderly subjects with Alzheimer's disease, mild cognitive impairment, and normal cognition. *J Alzheimers Dis*. 2015;44(3):1023–1034.
24. Boutet C, Rouffange-Leclair L, Schneider F, Camdessanché JP, Antoine JC, Barral FG. Visual assessment of age-related white matter hyperintensities using FLAIR images at 3 T: inter- and intra-rater agreement. *Neurodegener Dis*. 2016;16(3–4):279–283.
25. Wahlund LO, Julin P, Johansson SE, Scheltens P. Visual rating and volumetry of the medial temporal lobe on magnetic resonance imaging in dementia: a comparative study. *J Neurol Neurosurg Psychiatry*. 2000;69(5):630–635.
26. Shen Q, Loewenstein DA, Potter E, et al. Volumetric and visual rating of magnetic resonance imaging scans in the diagnosis of amnesic mild cognitive impairment and Alzheimer's disease. *Alzheimers Dement*. 2011;7(4):e101–e108.
27. Mitnitski AB, Fallah N, Dean CB, Rockwood K. A multi-state model for the analysis of changes in cognitive scores over a fixed time interval. *Stat Methods Med Res*. 2014;23(3):244–256.
28. De Coene B, Hajnal JV, Gatehouse P, et al. MR of the brain using fluid-attenuated inversion recovery (FLAIR) pulse sequences. *AJNR Am J Neuroradiol*. 1992;13(6):1555–1564.
29. Tang MY, Chen TW, Zhang XM, Huang XH. GRE T2*-weighted MRI: principles and clinical applications. *Biomed Res Int*. 2014;2014:312142.
30. Jack CR Jr, Bernstein MA, Fox NC, et al. The Alzheimer's Disease Neuroimaging Initiative (ADNI): MRI methods. *J Magn Reson Imaging*. 2008;27(4):685–691.
31. Weiner MW, Aisen PS, Jack CR Jr, et al. The Alzheimer's disease neuroimaging initiative: progress report and future plans. *Alzheimers Dement*. 2010;6(3):202–211.e7.
32. Morris JC, Weintraub S, Chui HC, et al. The Uniform Data Set (UDS): clinical and cognitive variables and descriptive data from Alzheimer Disease Centers. *Alzheimer Dis Assoc Disord*. 2006;20(4):210–216.
33. Beekly DL, Ramos EM, Lee WW, et al; NIA Alzheimer's Disease Centers. The National Alzheimer's Coordinating Center (NACC) database: the Uniform Data Set. *Alzheimer Dis Assoc Disord*. 2007;21(3):249–258.
34. De Reuck J, Auger F, Durieux N, et al. Topography of cortical microbleeds in Alzheimer's disease with and without cerebral amyloid angiopathy: a post-mortem 7.0-tesla MRI Study. *Aging Dis*. 2015;6(6):437–443.
35. Urs R, Potter E, Barker W, et al. Visual rating system for assessing magnetic resonance images: a tool in the diagnosis of mild cognitive impairment and Alzheimer disease. *J Comput Assist Tomogr*. 2009;33(1):73–78.
36. Dallaire-Thérault C, Callahan BL, Potvin O, et al. Radiological-pathological correlation in Alzheimer's disease: systematic review of antemortem magnetic resonance imaging findings. *J Alzheimers Dis*. 2017;57(2):575–601.

Supplementary materials

A

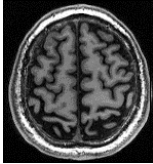
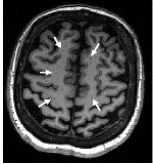
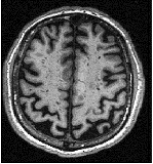
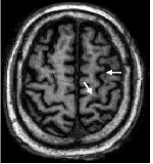

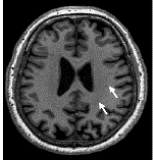

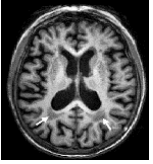
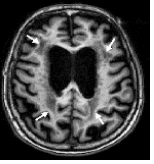
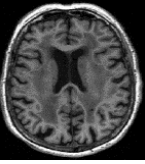
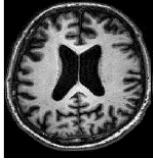
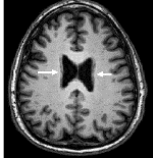

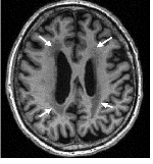
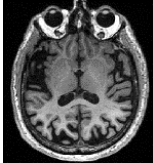
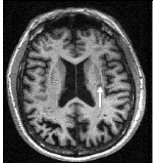
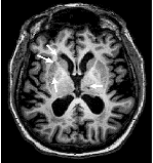
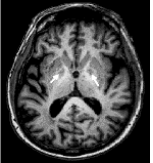
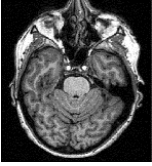
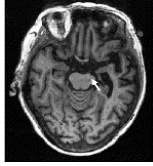
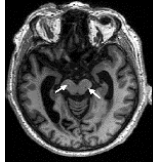
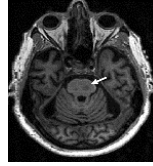
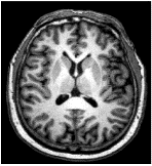
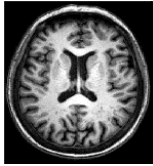
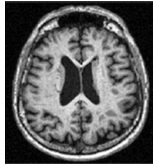
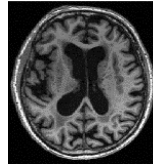
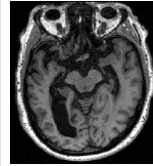
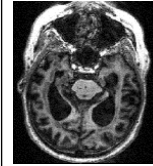
BALI category	Score					
	0	1	2	3	4	5
GM-SV Gray matter lesions and subcortical dilated perivascular spaces	Signal intensity is homogeneous in gray matter and subcortical areas	Dotted low signal intensity in gray matter, or multiple dotted/linear low signal intensities in subcortical areas	Small patches of low signal intensity in gray matter, or diffuse and countless dotted/linear low signal intensities in subcortical areas	Patches of low signal intensity in gray matter	—	—
					—	—
DWM Deep white matter lesions	Signal intensity is homogeneous in the deep white matter	Dotted low signal intensity in deep white matter	Small patchy low signal intensity lesions in deep white matter	Large patchy low signal intensity lesions in deep white matter	Large patchy low signal intensity lesions involving deep white matter in all cerebral lobes	Low signal intensity lesions involving all deep white matter
						
PV Periventricular white matter lesions	Signal intensity is homogeneous in periventricular white matter	Cap or shape low signal pencil thin line of low signal intensity in periventricular white matter	Patchy halo of low signal intensity with blurred margin in periventricular white matter	Patchy low signal intensity lesion connected with lesion in deep white matter	—	—
					—	—
BG Lesions in the basal ganglia and surrounding areas	Signal intensity is homogeneous in basal ganglia and surrounding areas regardless of dilated perivascular spaces	Only one dotted low signal intensity lesion in basal ganglia and surrounding areas regardless of dilated perivascular spaces	More than one dotted low signal intensity lesion in basal ganglia and surrounding areas regardless of dilated perivascular spaces	Patchy low signal intensity lesion in basal ganglia and surrounding areas regardless of dilated perivascular spaces	—	—
					—	—

Figure S1 (Continued)

IT Lesions in the infratentorial regions	Signal intensity is homogenous in the infratentorial regions	Only one dotted low signal intensity lesion in the infratentorial regions	More than one dotted low signal intensity lesion in the infratentorial regions	Patchy low signal intensity lesion in the infratentorial regions	—	—
					—	—
GA Global atrophy	No enlargement of ventricles and no widening of sulci	Mild enlargement of ventricles and widening of sulci	Moderate enlargement of ventricles and widening of sulci	Severe enlargement of ventricles and widening of sulci	Most severe atrophy present, especially in the medial temporal lobes	Most severe atrophy present in both medial temporal lobes and cerebral cortices
						

B

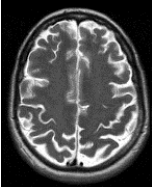
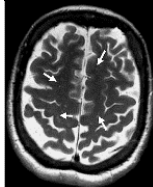
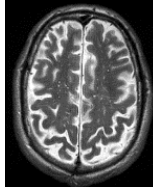
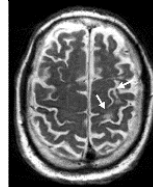
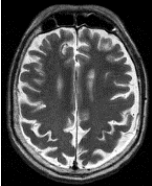
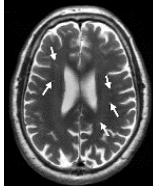

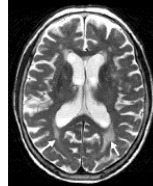
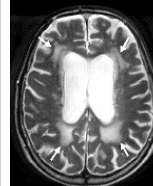
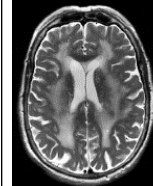
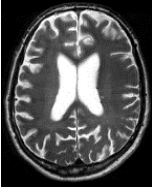
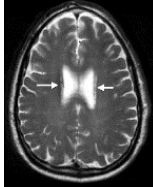
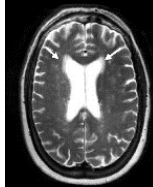
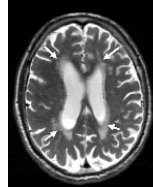
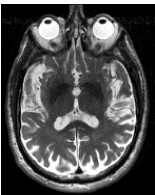
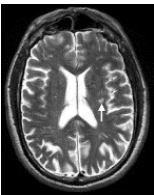
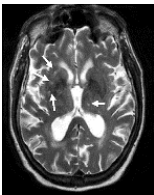
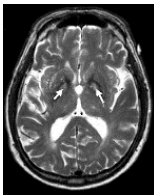
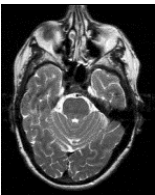
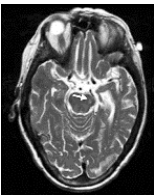
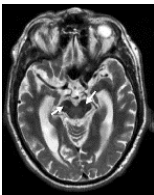
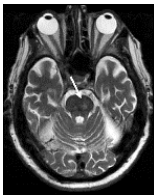
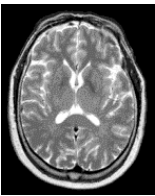
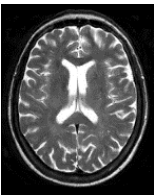
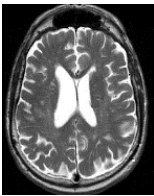
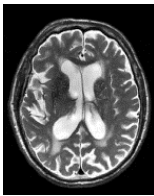
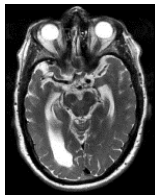
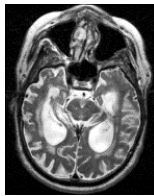
BALI category	Score					
	0	1	2	3	4	5
GM-SV Gray matter lesions and subcortical dilated perivascular spaces	Signal intensity is homogenous in gray matter and subcortical areas	Dotted high signal intensity in gray matter, or multiple dotted/linear high signal intensities in subcortical areas	Small patches of high signal intensity in gray matter, or diffuse and countless dotted/linear high signal intensities in subcortical areas	Patches of high signal intensity in gray matter	—	—
					—	—
DWM Deep white matter lesions	Signal intensity is homogenous in the deep white matter	Dotted high signal intensity in deep white matter	Small patchy high signal intensity lesions in deep white matter	Large patchy high signal intensity lesions in deep white matter	Large patchy high signal intensity lesions involving deep white matter in all cerebral lobes	High signal intensity lesions involving all deep white matter
						
PV Periventricular white matter lesions	Signal intensity is homogenous in periventricular white matter	Cap or pencil thin line of high signal intensity signal in periventricular white matter	Patchy halo of high signal intensity with blurred margin in periventricular white matter	Patchy high signal intensity lesion connected with lesion in deep white matter	—	—
					—	—

Figure S1 (Continued)

BG Lesions in the basal ganglia and surrounding areas	Signal intensity is homogeneous in basal ganglia and surrounding areas regardless of dilated perivascular spaces	Only one dotted high signal intensity lesion in basal ganglia and surrounding areas regardless of dilated perivascular spaces	More than one dotted high signal intensity lesion in basal ganglia and surrounding areas regardless of dilated perivascular spaces	Patchy high signal intensity lesion in basal ganglia and surrounding areas regardless of dilated perivascular spaces	—	—
					—	—
IT Lesions in the infratentorial regions	Signal intensity is homogeneous in the infratentorial regions	Only one dotted high signal intensity lesion in the infratentorial regions	More than one dotted high signal intensity lesion in the infratentorial regions	Patchy high signal intensity lesion in the infratentorial regions	—	—
					—	—
GA Global atrophy	No enlargement of ventricles and no widening of sulci	Mild enlargement of ventricles and widening of sulci	Moderate enlargement of ventricles and widening of sulci	Severe enlargement of ventricles and widening of sulci	Most severe atrophy present especially in the medial temporal lobes	Most severe atrophy present in both medial temporal lobes and cerebral cortices
						

C

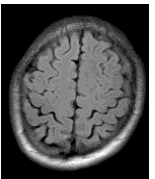
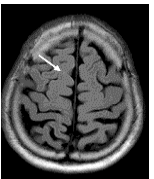
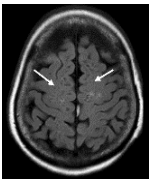
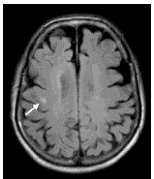
BALI category	Score					
	0	1	2	3	4	5
GM-SV Gray matter lesions and subcortical dilated perivascular spaces	Signal intensity is homogeneous in gray matter and subcortical areas	Dotted high signal intensity in gray matter, or multiple dotted/linear low signal intensities in subcortical areas	Small patches of high signal intensity in gray matter, or diffuse and countless dotted/linear low signal intensities in subcortical areas	Patches of high signal intensity in gray matter	—	—
					—	—

Figure S1 (Continued)

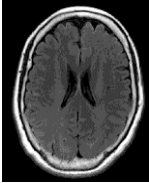

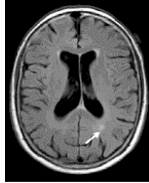
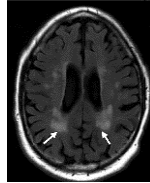
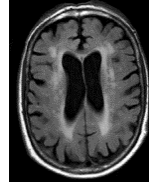
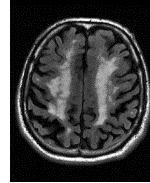
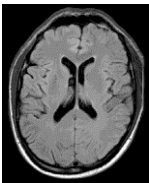
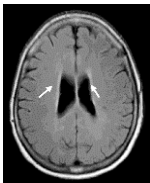
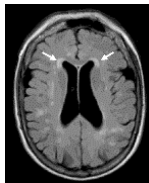
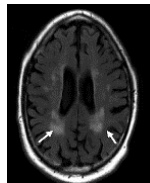
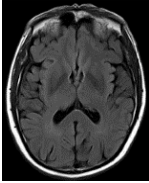
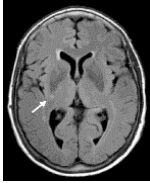


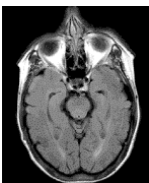
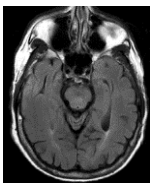
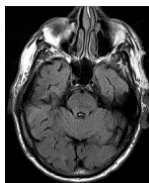
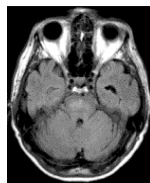
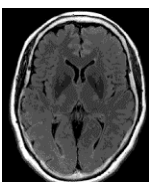


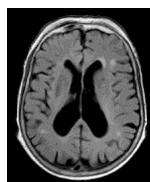
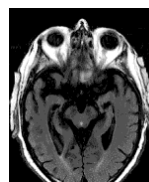
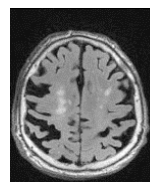
DWM Deep white matter lesions	Signal intensity is homogeneous in the deep and subcortical white matter	Dotted high signal intensity in deep and subcortical white matter	Small patchy high signal intensity lesions in deep and subcortical white matter	Large patchy high signal intensity lesions in deep and subcortical white matter	Large patchy high signal intensity lesions involving deep white matter in all cerebral lobes	High signal intensity lesion involving all deep white matter
						
PV Periventricular white matter lesions	Extremely thin line high signal intensity in periventricular white matter	Cap or pencil line shaped high signal intensity in periventricular white matter	Patchy halo of high signal intensity with blurred margin in periventricular white matter	Patchy high signal intensity lesion connected with lesion in deep white matter	—	—
					—	—
BG Lesions in the basal ganglia and surrounding areas	Signal intensity is homogeneous in basal ganglia and surrounding areas regardless of dilated perivascular spaces	Only one dotted high signal intensity lesion in basal ganglia and surrounding areas regardless of dilated perivascular spaces	More than one dotted high signal intensity lesion in basal ganglia and surrounding areas regardless of dilated perivascular spaces	Patchy high signal intensity lesion in basal ganglia and surrounding areas regardless of dilated perivascular spaces	—	—
					—	—
IT Lesions in the infratentorial regions	Signal intensity is homogeneous in the infratentorial regions	Only one dotted high signal intensity lesion in the infratentorial regions	More than one dotted high signal intensity lesion in the infratentorial regions	Patchy high signal intensity lesion in the infratentorial regions	—	—
					—	—
GA Global atrophy	No enlargement of ventricles and no widening of sulci	Mild enlargement of ventricles and widening of sulci	Moderate enlargement of ventricles and widening of sulci	Severe enlargement of ventricles and widening of sulci	Most severe atrophy present especially in the medial temporal lobes	Most severe atrophy present in both medial temporal lobes and cerebral cortices
						

Figure S1 (Continued)

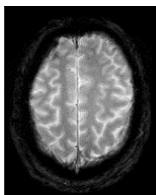
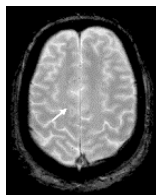
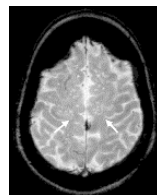
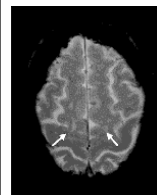
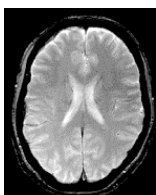
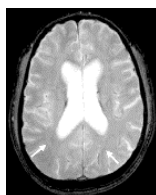
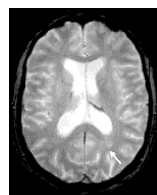
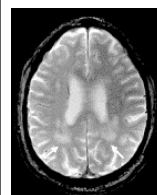
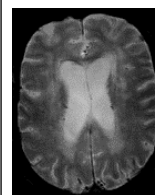
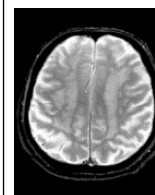
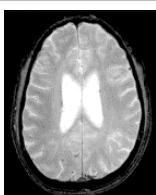
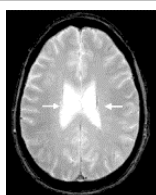
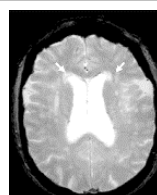
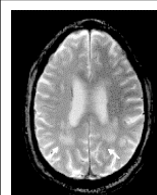
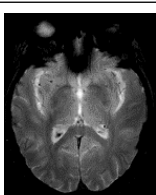
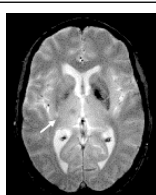
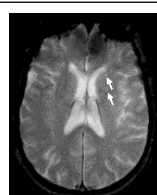
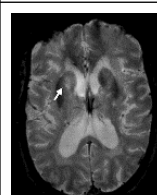
D	BALI category	Score				
		0	1	2	3	4
GM-SV Gray matter lesions and subcortical dilated perivascular spaces	Signal intensity is homogeneous in gray matter and subcortical areas	Dotted high signal intensity in gray matter, or multiple dotted/linear high signal intensities in subcortical areas	Small patches of high signal intensity in gray matter, or diffuse and countless dotted/linear high signal intensities in subcortical areas	Patches of high intensity in gray matter	—	—
					—	—
DWM Deep white matter lesions	Signal intensity is homogeneous in the deep and subcortical white matter	Dotted high signal intensity in deep and subcortical white matter	Small patchy high signal intensity lesions in deep and subcortical white matter	Large patchy high signal intensity lesions in deep and subcortical white matter	Large patchy high signal intensity lesions involving deep white matter in all cerebral lobes	High signal intensity lesion involving all deep white matter
						
PV Periventricular WM lesions	Signal intensity is homogeneous in periventricular white matter	Cap or pencil line shaped high signal intensity in periventricular white matter	Patchy halo of high signal intensity with blurred margin in periventricular white matter	Patchy high signal intensity lesion connected with lesion in deep white matter	—	—
					—	—
BG Lesions in the basal ganglia and surrounding areas	Signal intensity is homogeneous in basal ganglia and surrounding areas regardless of dilated perivascular spaces	Only one dotted high signal intensity lesion in basal ganglia and surrounding areas regardless of dilated perivascular spaces	More than one dotted high signal intensity lesion in basal ganglia and surrounding areas regardless of dilated perivascular spaces	Patchy high signal intensity lesion in basal ganglia and surrounding areas regardless of dilated perivascular spaces	—	—
					—	—

Figure S1 (Continued)

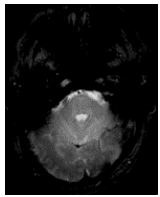
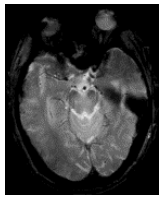
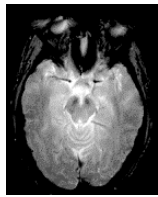
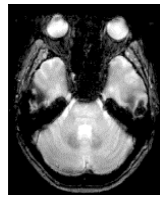
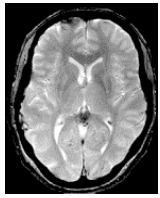
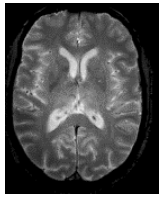
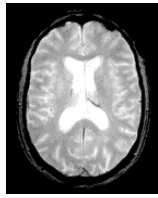

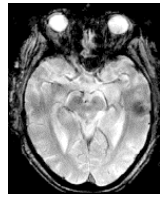
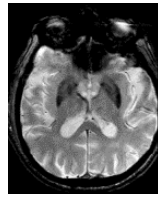
IT Lesions in the infratentorial regions	Signal intensity is homogeneous in the infratentorial regions	Only one dotted high signal intensity lesion in the infratentorial regions	More than one dotted high signal intensity lesion in the infratentorial regions	Patchy high signal intensity lesion in the infratentorial regions	—	—
					—	—
GA Global atrophy	No enlargement of ventricles and no widening of sulci	Mild enlargement of ventricles and widening of sulci	Moderate enlargement of ventricles and widening of sulci	Severe enlargement of ventricles and widening of sulci	Most severe atrophy present especially in the medial temporal lobes	Most severe atrophy present in both medial temporal lobes and cerebral cortices
						

Figure S1 Evaluation of the BALI based on T1WI (A), T2WI (B), T2-FLAIR (C), and T2*GRE (D).

Abbreviations: BALI, brain atrophy and lesion index; DWM, deep white matter lesions; GM-SV, gray matter, and subcortical lesions – subcortical dilated perivascular spaces; PV, periventricular white matter lesions; T2-FLAIR, T2-weighted fluid attenuated inversion recovery; T2*GRE, T2*-weighted gradient-recalled echo; T1WI, T1-weighted image; T2WI, T2-weighted image.

Table S1 A brief description of the four routine clinical sequences used for the BALI assessment

Sequence	Definition	General application	Chief features	Signal intensity characteristics		
				Gray matter and white matter	CSF	Common lesions
3D-T1WI	High-resolution 3D T1-weighted imaging using spoiled fast gradient echoes for acquisition during inversion recovery	Visualizing normal anatomy especially small details in three dimensions to improve delineation of GM and WM	TR >2,000 ms TE <5 ms TI 400–1,100 ms FA 7°–11°	GM lower SI than WM	Dark	Dark (fluid) Bright (paramagnetic substance)
T2WI	T2-weighted imaging highlighting differences in the T2 (spin–spin) relaxation time of tissues	Visualizing pathology	TR >2,000 ms TE >60 ms	GM higher SI than WM	Bright	Bright (fluid) Dark (paramagnetic substance)
T2-FLAIR	T2-weighted fluid attenuation inversion recovery sequence; signal intensity of free fluid was suppressed and removed by T1	Visualizing changes contained combined fluid for detecting subtle changes at the periphery of hemispheres and in periventricular regions	TR >2,000 ms TE >60 ms TI =2,000 ms	GM slightly higher SI than WM	Dark	Bright (combined fluid)
T2*GRE	T2*-weighted gradient recalled echo; susceptible to static field in homogeneities to detect the smallest changes in magnet field uniformity	Visualizing changes with susceptibility characters (paramagnetic substance deposition, similar to iron deposition or calcification)	TR 650–800 ms TE 3–20 ms FA 5°–20°	GM slightly higher SI than WM	Bright	Dark (eg, hemorrhage, calcification)

Abbreviations: 3D, three-dimensional; BALI, brain atrophy and lesion index; CSF, cerebral spinal fluid; FA, flip angle; GM, gray matter; SI, signal intensity; T1WI, T1-weighted image; T2WI, T2-weighted image; T2-FLAIR, T2-weighted fluid attenuation inversion recovery sequence; T2*GRE, T2*-weighted gradient recalled echo sequence; TE, echo time; TI, time of inversion; TR, repetition time; WM, white matter.

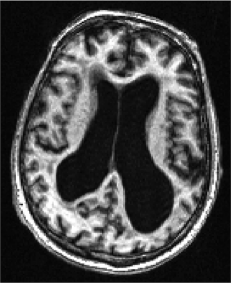
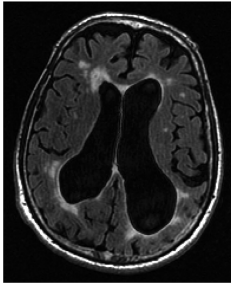
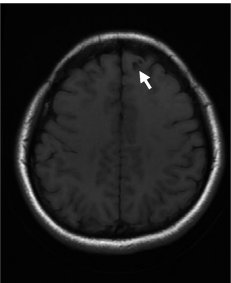
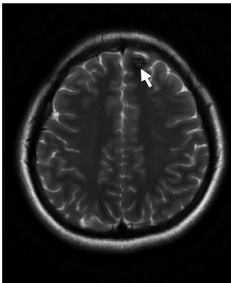
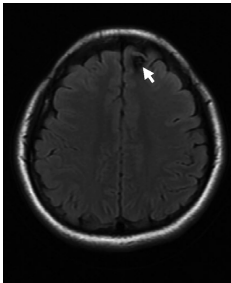
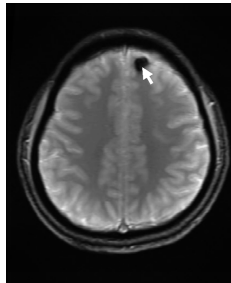
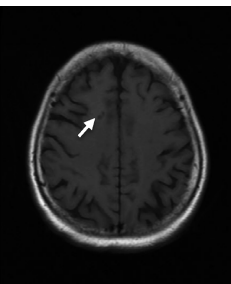
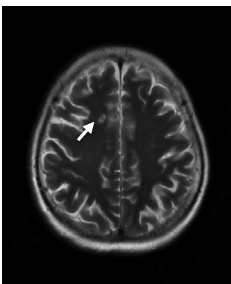
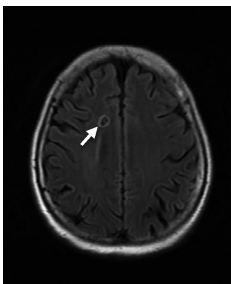
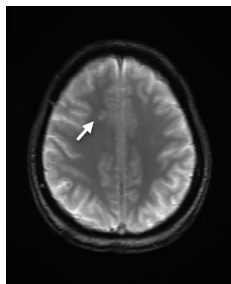
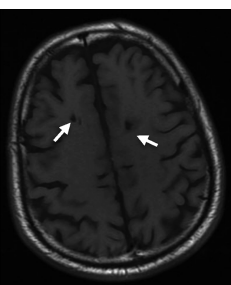
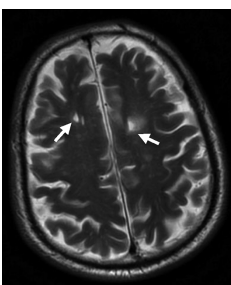
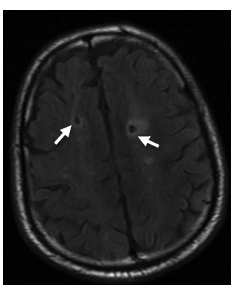
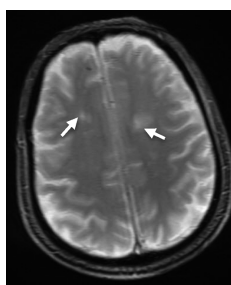
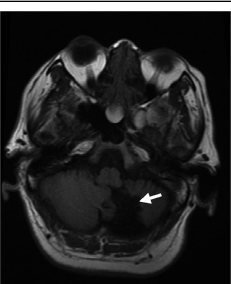
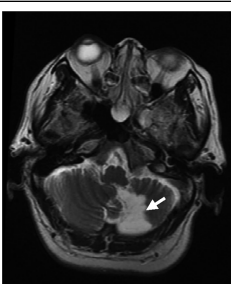
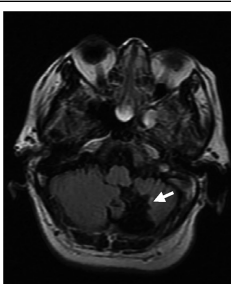
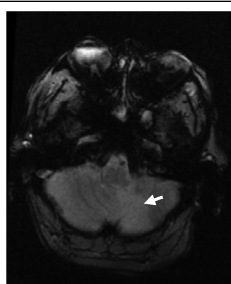
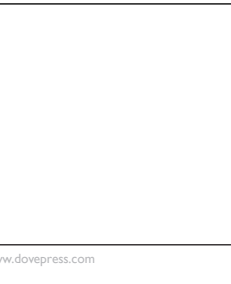



The “Others” category		Sequence			
		T1WI	T2WI	T2-FLAIR	T2*GRE
A	Normal pressure hydrocephalus				
B	Cavernous malformation				
Malacia	Single lacunar malacia				
	Multiple lacunar malacia				
Malacia	Malacia				
	Malacia				

Figure S2 (Continued)

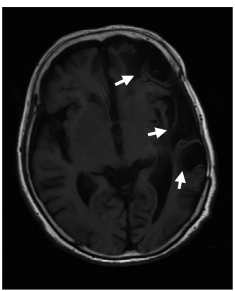
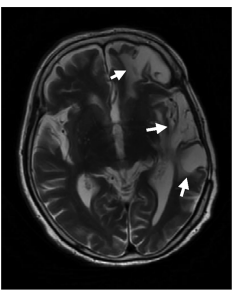
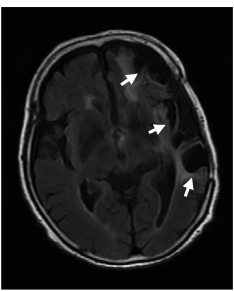
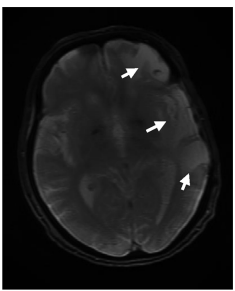
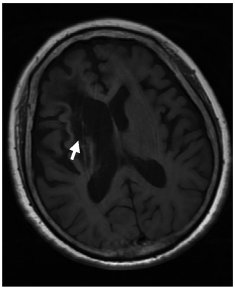
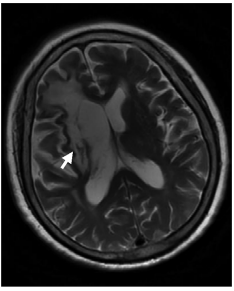
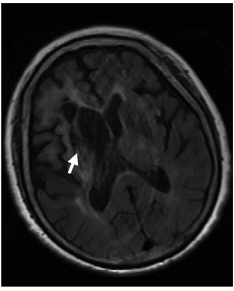
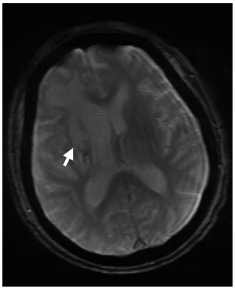
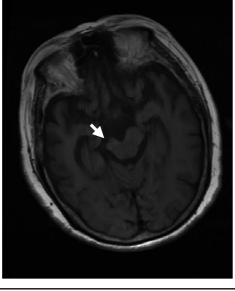
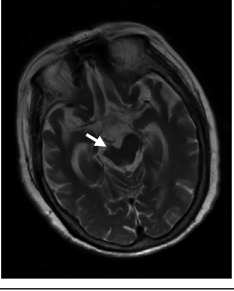
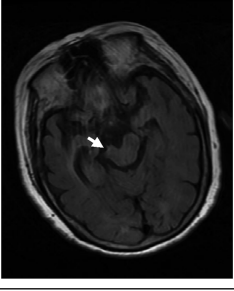
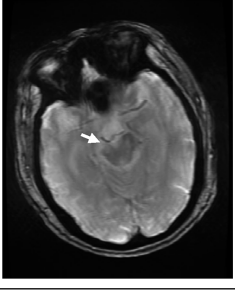
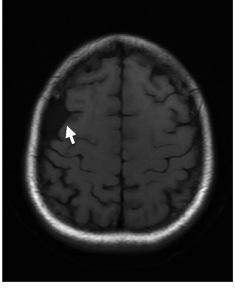
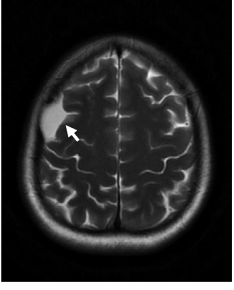
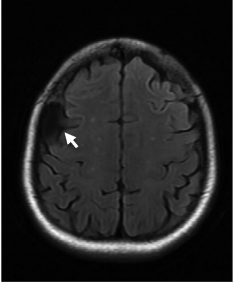
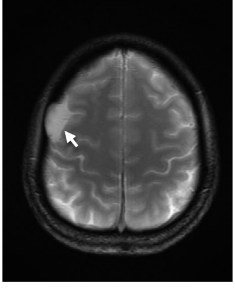
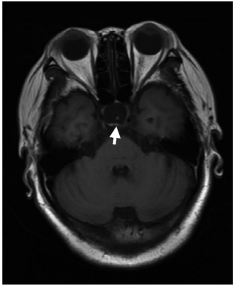

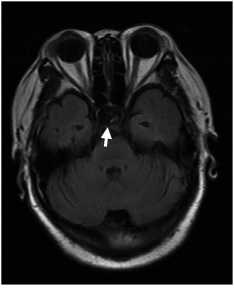
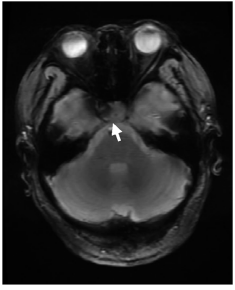
Malacia	Multiple malacia				
	Malacia with Wallerian degeneration				
					
	D Arachnoid cyst				
	E Empty sella				

Figure S2 (Continued)

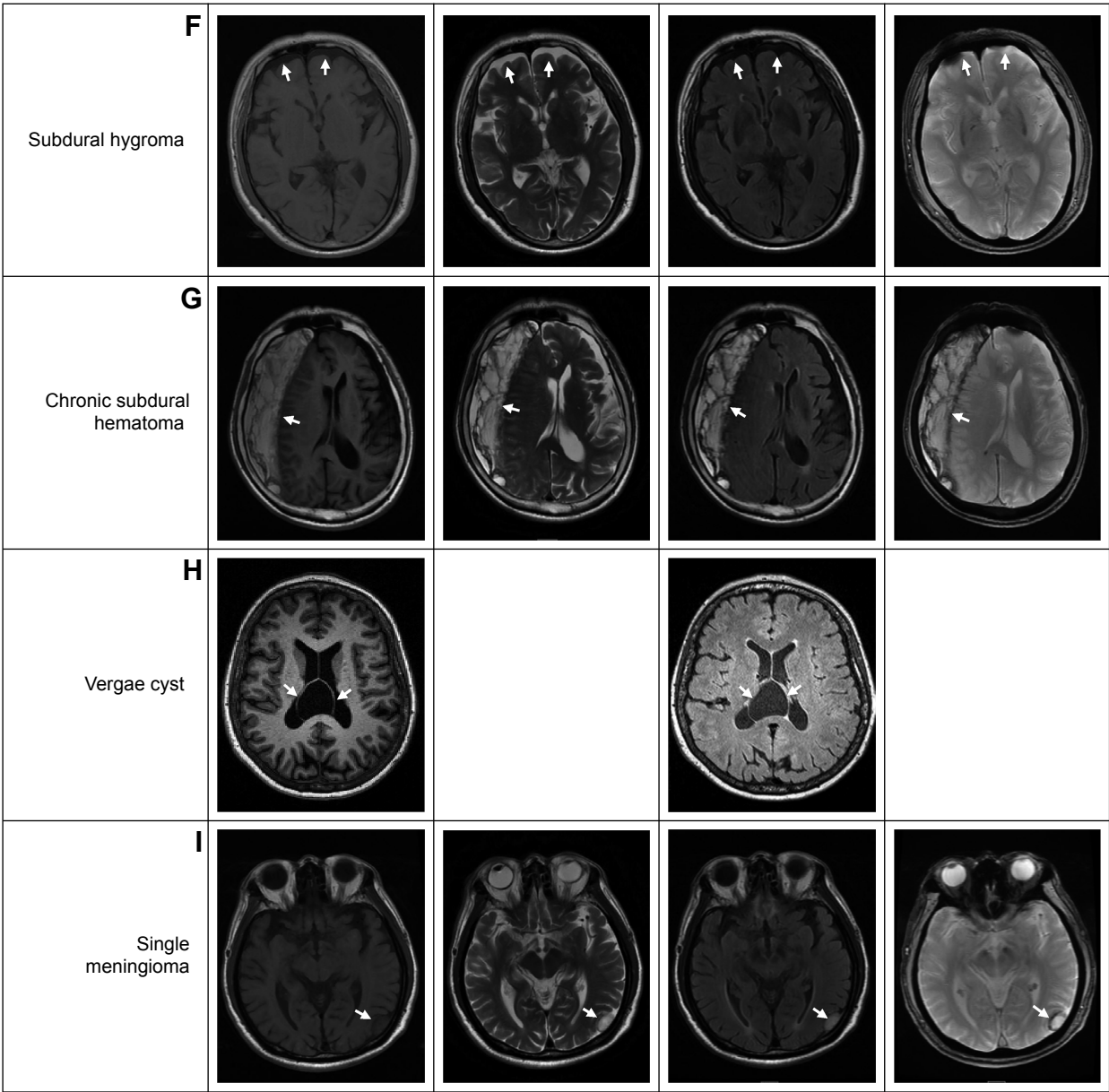


Figure S2 Examples of changes considered in the “Others” category of BALI evaluation, as seen on the appropriate sequences.
Abbreviations: BALI, brain atrophy and lesion index; T1WI, T1-weighted image; T2WI, T2-weighted image; T2-FLAIR, T2-weighted fluid attenuation inversion recovery sequence; T2*GRE, T2* weighted gradient recalled echo sequence.

Clinical Interventions in Aging

Dovepress

Publish your work in this journal

Clinical Interventions in Aging is an international, peer-reviewed journal focusing on evidence-based reports on the value or lack thereof of treatments intended to prevent or delay the onset of maladaptive correlates of aging in human beings. This journal is indexed on PubMed Central, MedLine,

CAS, Scopus and the Elsevier Bibliographic databases. The manuscript management system is completely online and includes a very quick and fair peer-review system, which is all easy to use. Visit <http://www.dovepress.com/testimonials.php> to read real quotes from published authors.

Submit your manuscript here: <http://www.dovepress.com/clinical-interventions-in-aging-journal>